Accepted Manuscript

Hybrid phase field simulation of dynamic crack propagation in functionally graded glass-filled epoxy

Duc Hong Doan, Tinh Quoc Bui, Nguyen Dinh Duc, Kazuyoshi Fushinobu

PII: S1359-8368(16)30912-X

DOI: 10.1016/j.compositesb.2016.06.016

Reference: JCOMB 4361

To appear in: *Composites Part B*

Received Date: 14 March 2016

Revised Date: 25 May 2016

Accepted Date: 3 June 2016

Please cite this article as: Doan DH, Bui TQ, Duc ND, Fushinobu K, Hybrid phase field simulation of dynamic crack propagation in functionally graded glass-filled epoxy, *Composites Part B* (2016), doi: 10.1016/j.compositesb.2016.06.016.

Hybrid Phase Field Simulation of Dynamic Crack Propagation in Functionally Graded Glass-Filled Epoxy

Duc Hong Doan[1,4*], Tinh Quoc Bui[2,3,*], Nguyen Dinh Duc[4], Kazuyoshi Fushinobu[1]

[1]Department of Mechanical and Control Engineering, Tokyo Institute of Technology, 2-12-1, Ookayama, Meguro-ku, Tokyo 152-8552 Japan

[2]Institute for Research and Development, Duy Tan University, Da Nang City, Vietnam

[3]Department of Civil and Environmental Engineering, Tokyo Institute of Technology, 2-12-1-W8-22, Ookayama, Meguro-ku, Tokyo 152-8552 Japan

[4]Advances Materials and Structures Laboratory, University of Engineering and Technology, Vietnam National University, Hanoi, 144 Xuan Thuy, Cau Giay, Hanoi, Vietnam

[*]Corresponding authors
Tels.: +81-(0)3-5734-2945 (D. H. Doan); +81-7021506399 (T. Q. Bui)
Email: doan.d.aa.eng@gmail.com (D.H.Doan); buiquoctinh@duytan.edu.vn; tinh.buiquoc@gmail.com (T. Q. Bui)

Abstract

Numerical simulation of dynamic crack propagation in functionally graded glass-filled epoxy (FG) beams using a regularized variational formulation is presented. The Griffith's theory based hybrid phase field approach for diffusive fracture is taken, which is able to accurately simulate complex behaviors of dynamic crack growth in FGMs. The FG beams under impact loads experimented by Kirugulige and Tippur (Exper. Mech. 2006; 46:269-281) are considered, taking the same configurations, material property, crack location, and other relevant assumptions. The crack paths, crack length, crack velocity, energies, etc., computed through the hybrid phase field model are numerically analyzed, and some of those results are directly compared with the experimental data. Due to lack of necessary information regarding impact loading profiles and boundary conditions in setting the tests, the simulations become difficult as an inappropriate definition of loading and boundary conditions can significantly alter the outputs of numerical solutions. This issue is important and thus is discussed. Two specific loading profiles, the constant and the linear displacement velocities, are taken into account, while free-free FG beams are considered. We show that good agreements of crack paths between the experiment and phase field approaches can be obtained. Numerical results also confirm a significant effect of elastic gradients on final crack paths. Similar to the experimental results, we also found that the crack path kinks significantly when situated on the stiffer side compared to the compliant side of the FG specimen.

Keywords: B. Fracture; B. Impact behaviour; C. Computational modelling; C. Damage mechanics; phase field model; dynamic crack growth; functionally graded materials.

1. Introduction

Advanced functionally graded materials (FGMs), which are known as a special composite material emerged recently, have been widely used in many engineering applications including aerospace, automotive, marine, civil engineering [1, 35-38]. The FGMs are characterized by spatially varying material properties with the goals, for instance, of reducing stress concentrations, relaxing residual stresses, or enhancing the bonding strength of composite constituents [2]. Typical applications of FGMs, as stated out in [3], include the impact resistant structures for ballistics and armors, thermal barrier coatings in high temperature components, interlayers in microelectronic packages, and many others. The most distinctive features of FGMs over constituent materials are that the compositions and volume fractions of the constituents in FGMs are varied gradually, thus resulting in a non-uniform microstructure in the material with continuously graded macro-properties as illustrated in Fig. 1 [4]. The FGMs however are very brittle, and the extent to which these FGMs can be tailored against failure or damage becomes more important. The knowledge of fracture behaviors, especially the dynamic crack propagation in FGMs, which is being studied in this work, is hence essential in order to evaluate their integrity.

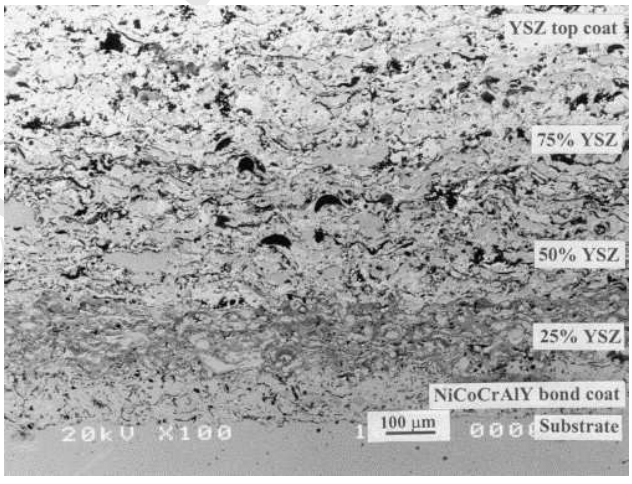

Fig. 1 Non-uniform microscopically inhomogeneous structure of the NiCoCrAlY-YSZ composite five layered functionally graded material [4].

Numerical failure mechanism simulation of dynamic crack propagation in FGMs remains a significant challenge in computational mechanics. The capability to investigate fracture behaviors of FGMs under dynamic loading conditions is important to their effective design and development. While static analysis offers designers and engineers with an indication of critical state of the stress contribution in a cracked body, real world structures, however, are invariably loaded dynamically. Most of previous works available in literature have dedicated to the determination of static fracture parameters and quasi-static crack growth simulation (see [5-8]), whereas studies accounting for dynamic crack propagation in FGMs are rather rare. Tippur and his co-workers [3, 9, 10] presented an interesting study of dynamic crack propagation in bending beams made of Soda-lime glass and epoxy materials. They mainly conducted an experimental procedure using optical method of Coherent Gradient Sensing and high-speed photography, while validated numerical results derived utilizing cohesive element and standard finite element method (FEM) have also been added. Yang et al. [11] investigated dynamic fracture of FGMs under impact loading using the FEM, considering the influence of non-homogeneity, loading ratio, and crack velocity. Notice that the mass density and Poisson's ratio have been assumed to be constant in [11]. Jain and Shukla [12] described a detailed analytical and experimental investigation to dynamic fracture of FGMs under mode I and mixed-mode loading conditions. Zhang and Paulino [13] developed a cohesive zone model integrated into a graded element formulation for dealing with dynamic failure processes in FGMs. They addressed an incorporation of a failure criterion into the cohesive zone model using both a finite cohesive strength and work to fracture in material description. In terms of cohesive method, Kandual et al. [14] presented an explicit cohesive volume finite element for dynamic fracture and wave propagation in FGMs. Very recently, Cheng et al. [15] introduced a peridynamic model, which is based on non-local continuum mechanics formulation eliminating spatial derivatives, to model dynamic fracture in FGMs. For curious readers, further information of dynamic fracture studies in FGMs can be found in an excellent review made by Shukla et al. [16].

Apart from the limitations of experimental works, existing numerical methods have also found very difficult or cumbersome in accurate simulations of fracture in FGMs, especially dynamic crack propagation. In the last decades, great efforts have put into the developments of effective, novel and accurate approaches for numerical simulation of dynamic fracture problems and an enormous achievement has been reached. The linear elastic fracture mechanics (LEFM) theory, which is based on Griffith's theory for brittle fracture, has successfully applied to solve a wide range of engineering problems. The underlying idea behind the Griffith's theory is to drive the crack nucleation and propagation by a critical value of the energy release rate [17]. In general, there are two major approaches that can be applied to the modeling of brittle fracture, the discrete and the smeared methods. Advances involved in terms of the discrete methods can be named as the local enriched partition-of-unity, see e.g., [18-21], embedded finite element method [22], cohesive crack model [10, 13, 14], etc., In this discrete setting, the discontinuities like crack are introduced and directly integrated in the displacement fields in the framework of the Griffith's theory and finite element method (FEM). The smeared methods like the classical continuum damage mechanics (see e.g., [23]), or a regularized phase field fracture model (see e.g., [24-27]), alternatively, are based on the energy minimization concept. Their aim is to incorporate a *damage variable* or to introduce a *fracture phase field parameter* into the model to describe the deterioration of materials or to let crack propagate along a path of least energy. More specifically, the phase field formulation, in contrast to the discrete fracture approach, drives the evolution of crack through the fracture phase field parameter, which is obtained by introducing a local history field containing a maximum energetic crack source in terms of deformation history. This definition allows one to update the field variables like the fracture phase field, displacements and history in a certain time step. Different versions of phase field models (i.e., physics and mechanics) have been classified clearly and can be found in [26], an excellent review work published recently. Nevertheless, the crucial idea of the phase field model is to indicate the cracks that should propagate along a path of least energy, as the minimizer of a global energy function, by which a phase parameter is introduced to track the

cracked and uncracked regions of the body [24]. One major advantage of this phase field approach is that the fracture problem is reformulated as a system of partial differential equations that completely determine the evolution of cracks, highly suitable for high gradients problems. There are neither phenomenological rules nor conditions needed to determine crack nucleation, growth or bifurcation. More importantly, the phase field models do not require any numerical tracking of discontinuities in the displacement fields. Consequently, the difficulties of discrete approaches in predicting *crack initiation* and *crack velocity* can now be overcome by using phase field methods [25, 26].

The phase field models have been applied to failure and damage analysis of homogeneous and non-homogeneous materials [26], while only a few works have dedicated to dynamic crack propagation in brittle and quasi-brittle materials, e.g., see [28-32]. The phase field simulation of dynamic crack propagation in FGMs made of Soda-lime glass and epoxy materials, however, has not been available in literature yet when this paper is being reported.

The main objectives of this work are fourfold: (a) to present and show an extension of the recently developed hybrid phase field model [26] and its applicability to the simulation of dynamic crack propagation in FGMs, exploring some major physical phenomena of dynamic fracture behaviors in FGMs, for instance, initial kink angles, crack initiation trend, crack velocity; (b) to rigorously and directly validate numerical crack path results with respect to the experimental data; (c) to numerically analyze the role and effect of the crack location, material gradation, impact loads and boundary conditions on the crack path; and (d) to address some numerical properties of the phase field model in dynamic fracture of FGMs and discuss some other relevant issues through the kinetic, fracture, and elastic energies.

It is worthy stressing out here that accurate simulations of dynamic crack propagation utilizing preceding numerical approaches is often difficult and challenging in some extent. It may be due to, for instance, the inherent non-homogeneous behavior and the lack of symmetry in material properties of FGMs. Further discussion on this issue can be found, for instance, in [13-15].

In this work, we are particularly interested in simulation of edge-notch bending glass-filled epoxy beams under offset impact loading as schematically depicted in Fig. 2, which were experimentally investigated by Kirugulige and Tippur [3]. The same geometry is taken for two configurations shown in Fig. 2, one FGM beam with a crack located on the stiffer side and the other with a crack located on the compliant side are numerically simulated. Similarly, we also take into account the homogeneous beam to further explore the difference in fracture behavior under dynamic loading due to functional grading. The homogeneous beam has all the features as the two FGMs beams except its material property. The crack paths, crack length, different types of loading, crack velocity, fracture energy, kinetic energy, elastic energy, etc., computed by the hybrid phase field model will be considered, investigated and validated against the experimental data in [3].

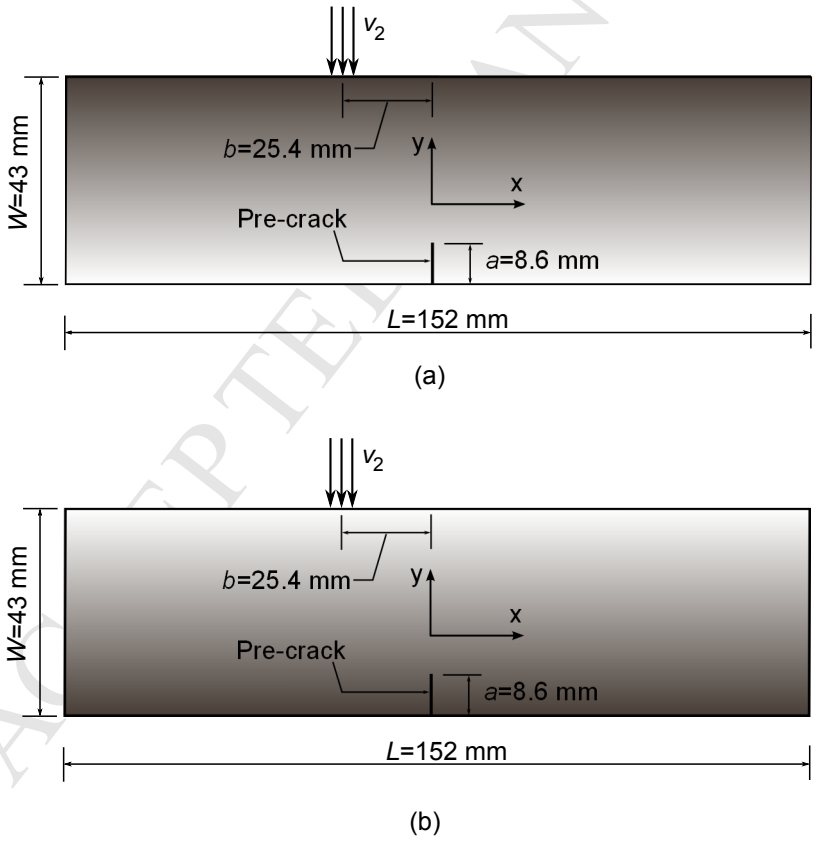

Fig. 2 Schematic of two configurations of FG beams and their geometry parameters: (a) FG beam with a crack located on the stiffer side; and (b) FG beam with a crack located on the compliant side. Our definition of the stiffer side and compliant one is exactly the same as that in [3].

In what follows, we briefly describe, in Section 2, the materials to be used for the simulation and solution procedure in the context of the hybrid phase field formulation, in which some important issues in regard of the implementation of the phase field approach will be presented. To accurately reproduce the experimental tests through numerical methods, an appropriate definition of loading and boundary conditions in the modeling is often required. An inappropriate definition of the loading or the boundary condition, of course, induces unacceptable outputs. In other words, the success of simulations totally depends on the aforementioned issues. To this end, this issue is discussed in Section 3. Subsequently, the numerical results and discussion will be given in Sections 4 and 5. Some conclusions drawn from the study are summarized in the last section.

2. Materials and solution method

We start by considering a mixed-mode experimental test of FGMs conducted by Kirugulige and Tippur [3]. The FGM beams are made of epoxy with continuously varying volume fraction of glass-filler particles, the Soda-lime glass, (35 μm mean diameter) from 0% to 40%. The material properties of FGMs are fitted from the experimental data [3], which are then shown in Figs. 3a, 3b and 3c where the density, elastic modulus and fracture energy continuously vary from the bottom side to the top of the FGM beams. Here, the dotted represent the real data reproduced from Kirugulige and Tippur [3], whereas the solid lines represent the fitting curves, which will be used in our simulation throughout the study. Notice that the corresponding Poisson's ratio variation between 0.33 and 0.37 mentioned in [3] was not expected to play a significant role in fracture behavior of FGMs. It is therefore set to be a constant 0.34 throughout this analysis. In addition, the variation of mode I crack initiation toughness versus Young's modulus shown in Fig. 3c given by [3] is also taken for the simulations.

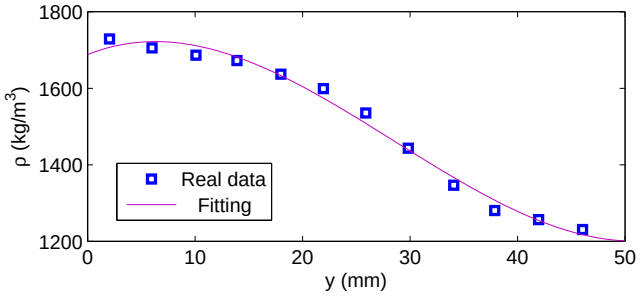

(a)

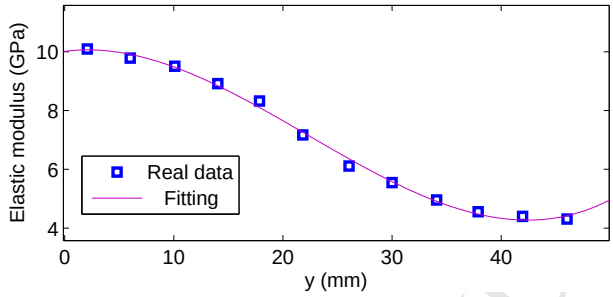

(b)

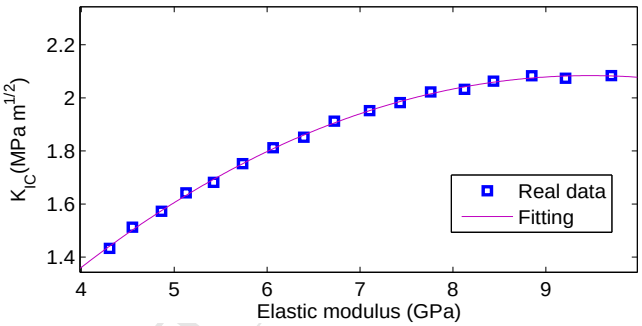

(c)

Fig. 3 Material properties of FGM beams. Variation of the density (a), the elastic modulus (b) and the fracture energy (c).

Regarding the solution method, we adopt the recently developed hybrid (isotropic-anisotropic) phase field model, which is proposed in [26] for brittle fracture, for our simulation purpose. The knowledge of standard momentum balance and the evolution equation of such hybrid fracture phase field formulation have already been detailed in [26]. We thus do not intend to repeat them here in this paper, for the sake of brevity. Instead, only the main idea of the hybrid phase field approach

with its evolution equation is briefly given, addressing some relevant important issues and versatile features of the method.

In terms of phase field fracture modeling [24-32], the cracks, which can be regarded as internal discontinuities with respect to the macroscopic field, are essentially represented by a phase field variable s bounded between 0 and 1. The phase field variable s varies continuously from 1 for undamaged materials to 0 for completely damaged materials. The hybrid (isotropic-anisotropic) phase field model for brittle fracture is finally formulated as follows [26]:

$$\begin{aligned} \sigma(\mathbf{u},s) &:= s^2 \frac{\partial \psi_0(\varepsilon)}{\partial \varepsilon} \\ l^2 \Delta s + (1-s) &= \frac{2l}{G_c} s H^+ \end{aligned} \tag{1}$$

where $\boldsymbol{\sigma}$, $\boldsymbol{\varepsilon}$ are the stress and strain tensors, respectively; $\mathbf{u}$ is the displacement field obeying the standard elastodynamic equation without damping effect $\rho\ddot{\mathbf{u}} = \mathrm{div}\sigma$, in which ρ is the mass density, div is the divergence operator, and the superposed dot represents the partial differentiation with respect to time. In Eq. (1), l stands for the length scale parameter introduced to account for the width of the crack. Further definition of the functional length scale parameter refers to, for instance, [25], and in this study, l=0.5 mm is selected. This length scale parameter is defined to control the gradient of the transition zone from damaged s=0 to undamaged s=1 materials. G_c denotes the material fracture toughness independent of the crack speed, Δs is the Laplacian of the phase field parameter, while H^+ introduces a strain history field of maximum positive reference energy, $\psi_0^+(\boldsymbol{\varepsilon})$, obtaining in a loading process, in order to handle the irreversibility of the crack phase field evolution [25]

$$H^+(\mathbf{x},t) := \max_{\tau \in [0,t]} \psi_0^+(\boldsymbol{\varepsilon}(\mathbf{x},\tau)) \tag{2}$$

By only applying the phase field parameter to the tensile part of the elastic energy density function, $\psi_0(\boldsymbol{\varepsilon})$, we thus prohibit crack propagation under compression, yielding

$$\psi_0^+(\boldsymbol{\varepsilon}) := \frac{1}{2}\lambda\langle tr(\boldsymbol{\varepsilon})\rangle_+^2 + \eta tr(\boldsymbol{\varepsilon}_+^2) \tag{3}$$

with the elastic constant $\lambda > 0$, $\langle tr(\boldsymbol{\varepsilon})\rangle_+ := \frac{1}{2}(tr(\boldsymbol{\varepsilon}) + |tr(\boldsymbol{\varepsilon})|)$, and $\eta > 0$ is the viscosity parameter. The evolution equation of the crack phase field is finally given by [25]

$$\eta\dot{s} = 2sH^+ + \frac{G_c}{l}\left((s-1) - l^2\Delta s\right) \tag{4}$$

where the superposed dot, $\dot{s}$, represents the partial differentiation of the phase field parameter with respect to time. In this study, the viscous term is neglected. In other words, by simply setting $\eta = 0$, the rate-independent evolution of the phase field parameter can be obtained [25, 26].

It is worth noting that, according to [26], there are two formulations of phase field approaches that can be treated as "basic" ones: the *isotropic* and the *anisotropic* formulations. The hybrid phase field model taken, however, contains advanced features of such two individuals. The underlying idea of the hybrid phase field model is to retain a linear momentum balance equation within a staggered scheme (i.e., a linear stress-strain relation), saving the computational time, while we still want the evolution of the phase field parameter s to be driven merely by the tensile elastic energy density, $\psi_0^+(\boldsymbol{\varepsilon})$, which is to avoid the cracking in the compressed domain [26].

Now, the evolution of crack is governed by the interplay between momentum balance and the evolution of the phase field. The kinetics of crack motion is restricted to fairly simple possibilities and the dynamics of fracture is based only on the interaction with momentum balance. In our work, a staggered iterative scheme is adopted to solve the resulting uncoupled equations [26]. The accuracy of this scheme in dynamic crack propagation of FGMs will be validated against the experimental data [3]. We then solve the resulting equations of motion in an effective way by using an in-house adaptive finite element method using 6-node quadratic triangular elements in

conjunction with a staggered iterative scheme. In this study, we used the anisotropic mesh refinement technique [43-44], in which a metric is employed to define the mesh size in each spatial direction. Generally, the interpolation error estimate is used in order to assess the metric. In this calculation, the metric is obtained from the interpolation error estimate of the phase-field parameter, which keeps a mesh to be fine enough in the damage area. Curious readers can refer to, for instance, Refs. [43-45] for more information.

Remark #1: It would be stressed out here that a small region represents a crack in terms of the phase field fracture approach in which the damage accumulates. This representation of the phase field in general is conceptually similar to the one employs within the context of continuum gradient damage theory, e.g., see [33]. Therefore, the phase field method could be viewed as a continuum gradient damage theory, but with a different way in derivation of the damage evolution equation.

3. Impact loading profiles and boundary conditions

We conduct two models of mixed-mode fracture experiments: (a) a pre-crack placed on the stiffer side of the beam with impact occurring on the compliant side, and (b) a pre-crack placed on the compliant side of the beam with impacting on the stiffer one. One of the underlying problems behind the simulations using the hybrid phase field approach is how to appropriately represent the impact loading and boundary conditions in the numerical implementation. This issue, as mentioned above, is important, and thus is discussed immediately.

As depicted in Fig. 2, the FGM specimens are rectangular beams that are initially set up with a pre-crack of 8.6 mm at the center of bottom side. A sudden loading on the top beam is applied by an impactor with a velocity of 5 m/s. In the reference [3], the description of impactor, unfortunately, is not adequately detailed to allow us to precisely prescribe an impact loading condition. The information of the rebound time and of the size of the hammer utilized as the impactor in the experiments is missed in [3]. Therefore, the impact loading profiles picked in this study are

assumed to be close to those used in the experiments, as much as possible. As a consequence, the impact loading condition is hence modeled as a displacement velocity with two different profiles, which are schematically depicted in Fig. 4a for a Heaviside step loading (termed as *a constant displacement velocity*) and Fig. 4b for a Heaviside step loading with a finite rise time (termed as *a linear displacement velocity*), for simplicity throughout the study.

$$u(t) = 5 : \text{Heaviside step loading}$$

$$u(t) = \begin{cases} 5t/t_0, t < t_0, t_0 = 300\mu s \\ 5, t \geq t_0 \end{cases} : \text{Heaviside step loading with a finite rise time} \quad (5)$$

Here, the constant displacement velocity implies that the top surface of FGM beam has the same mechanical impedance with the impactor. For the linear displacement velocity case, the top surface of FGM beam has, however, larger mechanical impedance than that of the impactor, and it takes a certain time in order to reach the set-up impact velocity of 5 m/s. The effect of these impact conditions will be examined in the numerical results.

Regarding the boundary conditions, we follow the original description applied to the experimental and FEM numerical simulation works by Kirugulige and Tippur [3, 10]. As pointed out in the reference works [3, 10] that while conducting experiments, the FGM beams are setup so that the specimens are initially rested on two blocks of soft putty, before imposing the impact load. They also addressed one important point that the main purpose of their set-up is to preclude or avoid any interaction from the support reactions, which may significantly alter the resulting dynamic fracture propagation behaviors. To this end, in our phase field simulation, the boundary conditions of the FGM beams are finally assumed to be free-free.

It is noticed that the free-free boundary conditions as shown in Fig. 2 use impact loading of the free beam since this was also taken the same in [10] for a FEM-based computational study. In the

present work, the **displacement** as a uniform distribution of the equivalent body force over a length of 1mm is applied on the top surface of specimen.

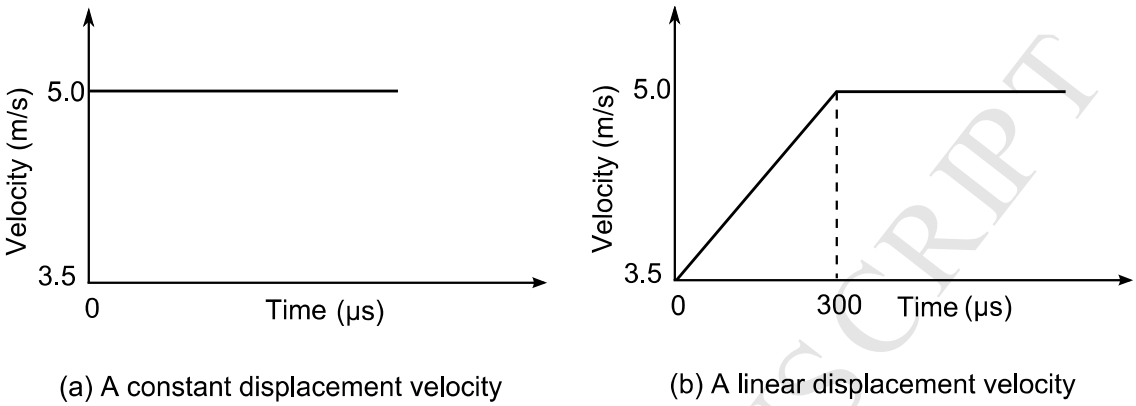

Fig. 4 Schematic of two impact loading profiles: (a) A constant displacement velocity (or a Heaviside step loading) and (b) a linear displacement velocity (or a Heaviside step loading with a finite rise time)

4. Numerical results of dynamic crack propagation

The first focus of our study is to show the capability of the hybrid phase field model in simulation of dynamic crack propagation in FGMs. Three edge-notch bending beams (two functionally graded glass-filled epoxy beams and one homogeneous beam) shown in Fig. 2 are considered. Note that the homogeneous beam (not show here) has exactly the same configuration to the two FG beams. The numerical computations are performed employing an in-house adaptive finite element approach with remeshing, integrating a staggered iterative scheme. All simulations using 6-node quadratic triangular elements for both displacements and phase field parameter are carried out with the material properties of FGMs sketched in Fig. 3. In Fig. 2, the specimens are subjected to an impact loading at an offset distance with respect to the initial crack location. A velocity of 5 m/s as explained above is thus specified to a small region composed of nodes at the impact location. All the simulations are performed under the plane stress state. The crack paths,

crack velocity, crack length, energies, etc., calculated by using the hybrid phase field model are investigated and compared with the experimental data [3].

Prior to analyzing the numerical results gained by the hybrid phase field formulation, it is necessary to address one important feature observed from the experimental works [3, 10]. To this end, Fig. 5 shows the final crack paths made by the experiment [3], provided that, as pointed out by Kirugulige and Tippur [3]: *"the differences in the crack paths are attributable directly to the combined effects of the elastic gradients as well as fracture toughness gradients"*. In other words, the final crack paths differ greatly for the two FGM beams. Another interesting point is that an initial kink angle of approximately 4° is found for the case under which the crack locates on the compliant side, while it is found for approximately 16° for the beam with the crack located on the stiffer side. Additionally, an initial kink angle of about 10° for the homogeneous beam is obtained, which is bounded by the ones for the two FGM beams. In what follows, we will verify these final crack paths through the hybrid phase field approach, and present and discuss some other relevant results.

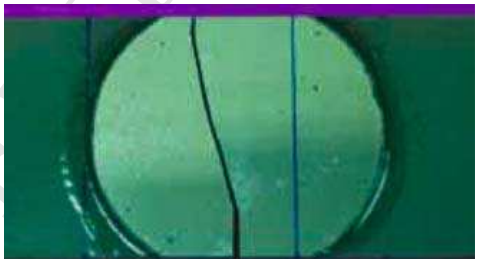

(a) An FGM beam with a crack located on the stiffer side

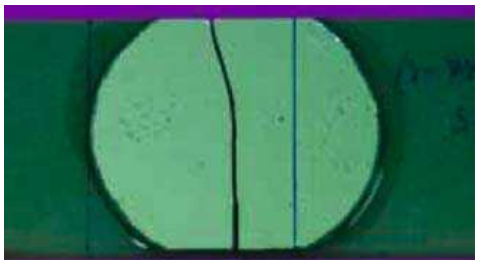

(b) An FGM beam with a crack located on the compliant side

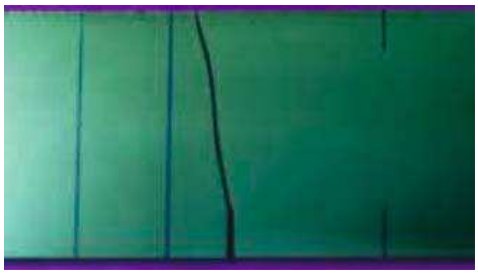

(c) A homogeneous beam

Fig. 5 Schematic of final crack paths (black solid lines) of two FGM beams (a), (b) and one homogeneous beam (c) made by the experiments [3]. A vertical line (marked in blue color) is located 10 mm away from the crack tip, which just helps to establish the scale.

4.1 Functionally graded beam with a crack located on the stiffer side

The first case is exactly concerned with the corresponding specimen shown in Fig. 2a, in which a pre-crack is fabricated to be placed on the stiffer side. It implies that the value of elastic modulus of the bottom side is larger than that of the top one. The hybrid phase field model is applied to calculate the dynamic crack growth of the specified FGM specimen. The computed result of the final crack path is then depicted in Fig. 6a showing the evolution graph of the phase field parameter. The constant displacement velocity sketched in Fig. 4a is used for this analysis. In Fig. 6a, the phase field parameter varies continuously from 0 (red region: damaged) to 1 (blue region: intact). Interestingly, in such figure a diffusive zone around the crack paths can also be seen, exactly reflecting the perspective of the phase field modeling. The final crack path computed by the hybrid phase field formulation matches well the experimental crack path data as seen in Fig. 6b. This excellent agreement in both solutions can be observed for the whole curves, i.e., from the initiation crack where the initial kink angles can be found to be identical. There is, however, a slight and insignificant difference at the very late stage of the final crack paths between two solutions. The discrepancy of crack paths at the very late stage of the final crack paths between experimental and computed results is attributed, for instance, to the assumed free-free boundary conditions at the

bottom of the model. Apart from the boundary condition, other reasons such as the stress wave, the finite size effect, etc., may also induce such a slight difference at the late stage of the final crack paths. Although the bottom face of the FGM specimen is experimentally assumed to be rested on two blocks of soft putty, in simulations, however, the assumption of free-free boundary condition to the bottom face of the beams may not completely be able to represent such two blocks of soft putty, and the effect of the reaction force induced by the support putty may lead to a certain level of errors of the final simulation results. In this case, as shown, the less accuracy can be found at the very late stage of the crack paths.

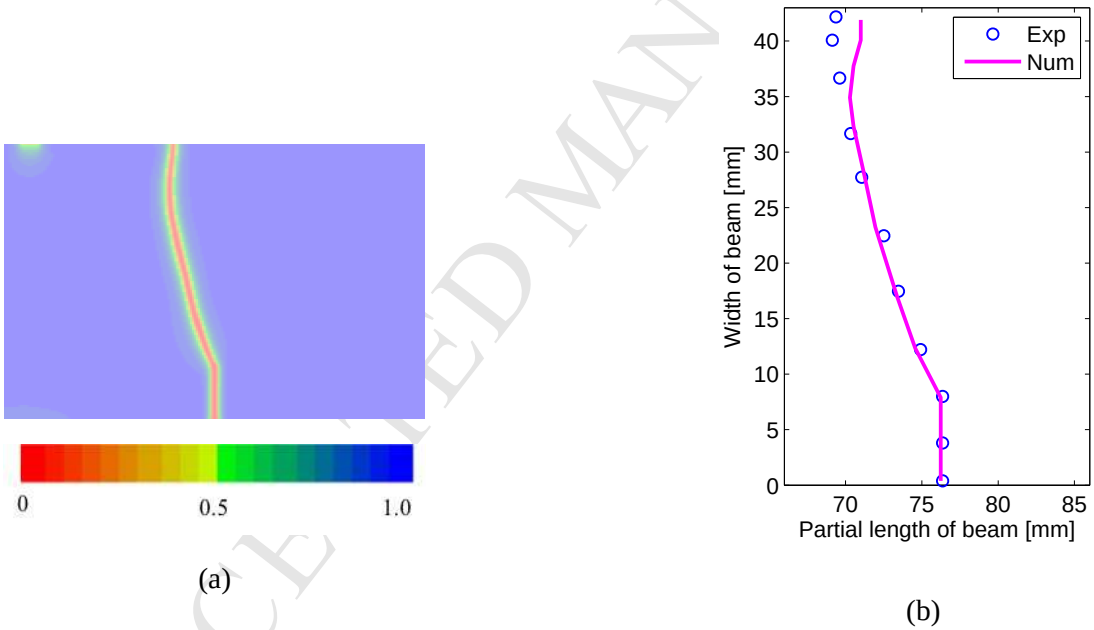

(a) (b)

Fig. 6 Comparison of the final crack paths (a) and (b) of an FGM beam with a crack located on the stiffer side obtained by the experiments [3] and the hybrid phase field formulation, taking the *constant* displacement velocity.

Fig. 7 shows the same numerical comparison between two approaches but the linear displacement velocity is taken into phase field implementation instead. In this particular case, the results indicate that by using the loading driven through the linear displacement velocity, the kink crack angle can be predicted well. A remarkable agreement of the crack paths between two solutions can also be obtained (crack paths grow up to half of the width of the specimen), but the

linear displacement velocity is not able to predict well for the full crack path, large error can be found at the late stage, see Fig. 7.

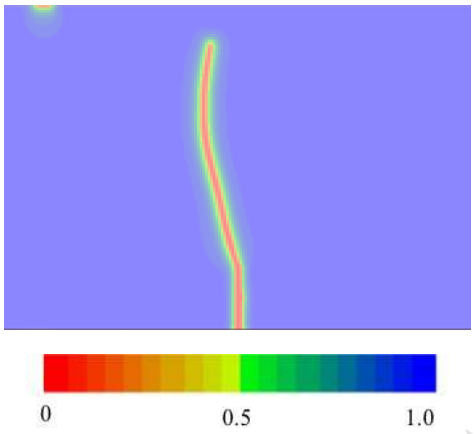

Fig. 7 Comparison of the final crack paths of an FGM beam with a crack located on the stiffer side obtained by the experiments [3] and the hybrid phase field formulation, taking the *linear* displacement velocity.

Next, the boundary conditions setting in dynamic crack propagation is important, which may affect the output numerical results of the simulation. The key point as already stressed out above is due to the fact that while the beams have been conducted experimentally supported on two blocks of soft putty, precluding the support reactions affecting the fracture behavior, in simulations however they are assumed to be free-free condition [3, 10]. We numerically show here that the free-free assumption could be applied to the simulations, but in fact that is not able to fully capture the real support conditions by the two soft putty blocks taken in the tests. Fig. 8 shows the deformation results of the FG beam at two different time steps calculated by the phase field model. We highlight one important point that can be observed from these deformation results that the effect of the support reaction on fracture behaviors is not small. In order words, the support reaction induced by the two blocks, in principle, can not be neglected. Specifically, the effect is significant at the late stage of the impact loading. At the early stage of loading, e.g., $t = 200\mu s$, the beam shown in Fig. 8a is being deformed. Here, attention must be focused on the bottom side of the beam at the two supports where the deformation is still small, but it becomes larger at the late stage of impact

loading, see Fig. 8b, e.g., $t = 320\mu s$, where the beam deforms unsymmetrically. It means that the support reaction realistically alters the fracture behavior, the crack paths. Therefore, the free-free beam assumption itself is possible for simulation, but not fully capture the real works of the experiments, a certain level of error can be reached. Therefore, it can be concluded that the less accuracy on the final crack paths at the late stage shown in Figs. 6c and 7b may be caused by this free-free boundary condition.

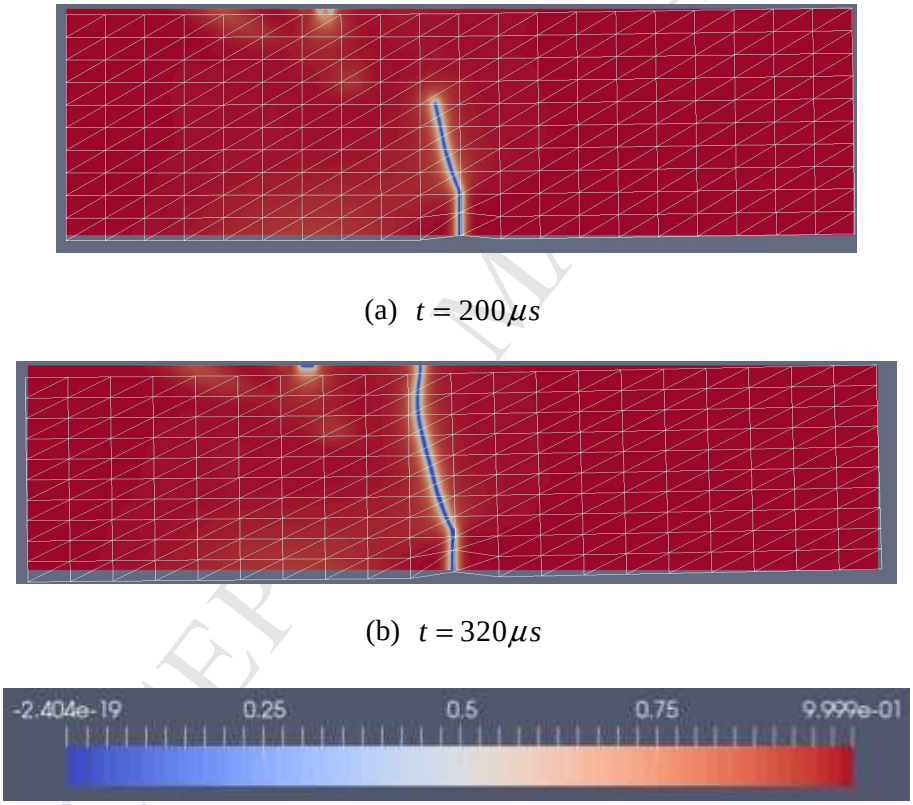

(a) $t = 200\mu s$

(b) $t = 320\mu s$

Fig. 8 Deformation of FG beams with a crack placed on the stiffer side at two different time steps, taking the *constant* displacement velocity. (red color represents the phase field, blue color represent the crack path)

Fig. 9 represents the evolution of crack length and crack velocity versus crack propagation time. Note that the crack propagation time defined is to measure the time when crack starts propagating. It is, on the other hand, to allow us to make a possible comparison between the simulation and the

test. In Fig. 9a, the solid line indicates the calculation result whilst the dots represent the experimental data reproduced from Kirugulige and Tippur [3]. It is apparent that a good agreement of the crack length versus crack propagation time between two solutions is obtained. The crack velocity with respect to crack propagation time obtained by the hybrid phase field model is also estimated and compared with that reproduced from the experimental data [3], see Fig. 9b. The amplitude of the crack velocity gained by two solutions is comparable (see dash-dot line).

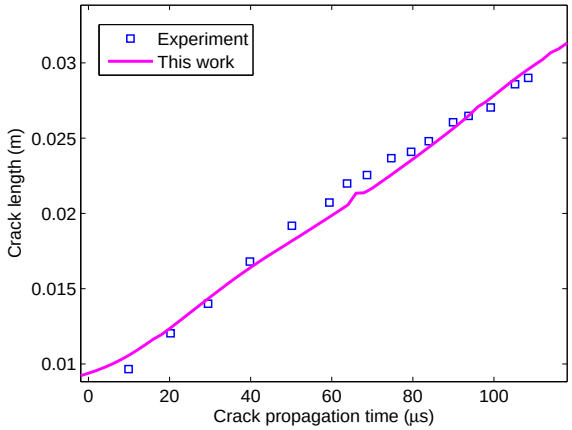

(a)

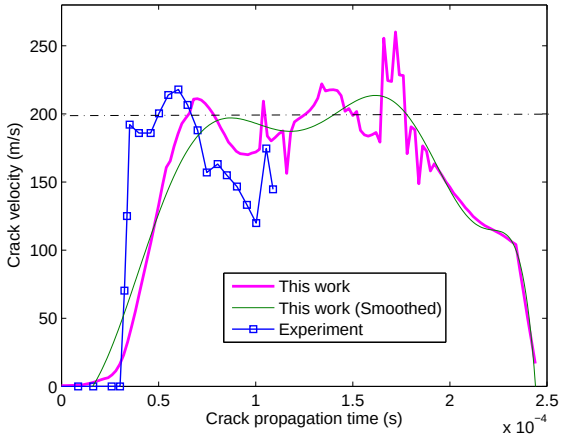

(b)

Fig. 9 FG beam with a crack located on stiffer side: Crack length versus crack propagation time (a) and crack velocity versus crack propagation time.

In terms of dynamic fracture analysis, the dynamic loading defined through the impact velocity plays a crucial role and may have effects on the fracture behaviors. To this end, two specified constant velocities of 3.5 m/s and 5 m/s are taken and their calculated results of crack paths accounted for the stiffer cracked specimen are shown in Fig. 10. The crack paths computed for two cases are completely different. Different impact velocities greatly alter the final crack paths. The higher velocity is imposed the larger the initial kink angle is gained. It is clear that the one suffering higher velocity grows faster than that of lower velocity. The resulting crack path of the higher velocity is longer that of the lower one.

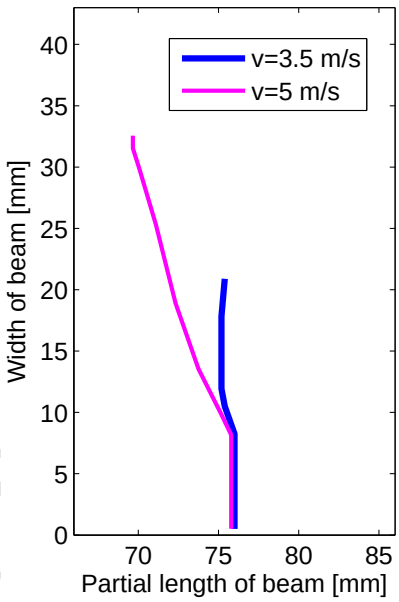

Fig. 10 Effect of different impact velocities on the crack paths and initial kink angles of stiffer cracked beams.

4.2 Functionally graded beam with a crack located on the compliant side

Next, we consider an FG beam with a pre-crack located on the compliant side (see Fig. 2b), in contrast to the previous stiffer beam. A pre-crack located on the compliant side means to serve lower elastic modulus. The hybrid phase field model taken is applied and the dynamic crack growth

of the FG specimen is then computed. Here, we are particularly interested in estimating the crack path, showing the evolution graph of the phase-field parameter. Fig. 11, as a consequence, depicts the resulting final crack paths calculated by the phase field model plotted altogether with the tests [3] for both the constant and linear displacement velocities. Overall, the calculation result with the linear displacement velocity shows a better agreement with experimental data than one with the constant displacement velocity. It can be seen even more in the crack path behavior that the model handling the constant displacement velocity is not able to produce the initial kink angle of the crack path. The crack path in this case immediately oscillates instead, and less accuracy compared with the experimental data is found. In the contrary, the initial kink angle can be captured well by the model taking the linear displacement velocity. The initial kink angle in this way matches well the experimental curve. However, the accuracy is found at the early stage only, large errors appear at the late stage of loading.

It is important to note here that both proposed loading profiles have been attempted but the final crack paths are unable to be reproduced accurately as compared with the experimental data. The main issue as already discussed above is that the necessary information of the loading profiles used for the real tests is missing in the reference work [3].

The constant and linear displacement velocities depend upon the model to be considered. In our numerical experiments, we find out that the model with a crack located on the stiffer side the constant displacement velocity offers better accuracy of the crack paths than that using the linear velocity support the hypothesis that top surface of FGM beam has the same mechanical impedance with the impactor. It is opposite when dealing with the beam with a crack located on the compliant side. In this case, the top surface of FGM beam has large density and elastic modulus than case of crack located on the stiffer side. It means that, the top surface of FGM beam has larger mechanical impedance than that of the impactor, and it takes a certain time in order to reach the set-up impact velocity of 5 m/s. In other words, the loading profiles are problem-dependent. It is reasonable since the loading profiles are a key factor in dynamic fracture analysis that controls the output of the final

solutions of problems. Therefore, the two loading profiles are attempted, in order to not only seek a reasonable result of the crack path, but also to exhibit the importance of loading conditions within the framework of dynamic fracture simulations.

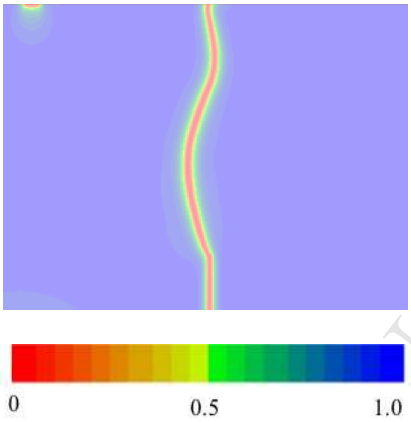

(a) Calculation result with the constant displacement velocity

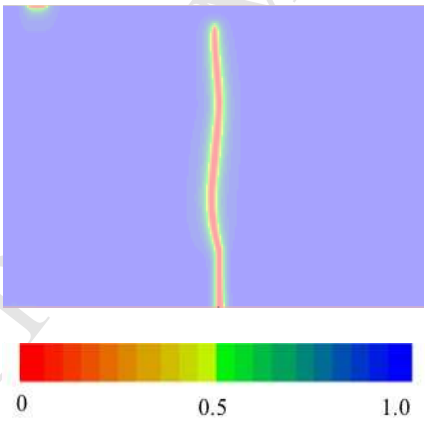

(b) Calculation result with the linear displacement velocity

Fig. 11 Comparison of final crack paths of an FG beam with a pre-crack located on the compliant side between the phase field method and experimental data.

4.3 A homogenous beam

In order to show the difference in fracture behavior due to functional grading of materials, a homogeneous beam is solved using the hybrid phase field model. The physical properties are: the

density ρ = 1175 kg/m^3, elastic modulus E = 3.2 GPa and K_{IC} = 1.26 MPa.m$^{1/2}$. The computed crack paths using the displacement velocity profiles in Fig. 4 are plotted in Fig. 12. Compared with the experimental data, the obtained result of crack paths with the constant displacement velocity shows better agreement than that employing the linear displacement velocity. Once again, less accuracy of the crack path at the late stage is found in this homogeneous case. The less accuracy may be caused by the boundary conditions. Nevertheless, both loading profiles can offer good initial kink angles.

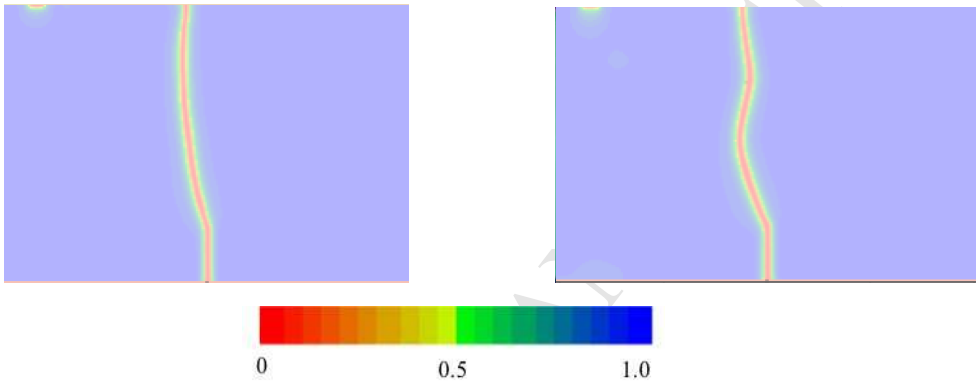

(a) Constant velocity (b) linear velocity

Fig. 12 Comparison of the final crack paths of a homogeneous beam between the numerical phase field model and experimental data: (a) constant and (b) displacement velocities.

5. Discussions

Three specimens of FG and homogeneous beams experimented by Kirugulige and Tippur [3] are numerically simulated by the hybrid phase field model. Obtained results apparently indicate the importance of impact loading profiles in simulation of dynamic fracture problems, which drive the crack paths. The two impact loading profiles proposed, without information from the tests, can be used for our phase field simulation, but the elastic gradient of materials greatly affect the final crack paths. Therefore, an appropriate choice of the impact loading profile should be considered for each model, in order to deliver a comparable result with the tests. Of course, the simulation will be more convenient and more feasible on the condition that detailed information in regard of the applied

loading profiles used for the tests is sufficiently provided. In that case, the numerical outputs could better fit the experimental data.

The boundary conditions are also found to be a critical factor altering the crack paths of the system. Obviously, the obtained numerical results exhibit an important role of the boundary conditions in dynamic fracture simulation. They indicate that the free-free boundary conditions are not able to fully capture the real boundary conditions of the two blocks of soft putty. The free-free boundary conditions could provide acceptable results but less accuracy of the crack paths at some parts takes place. Among three cases, boundary conditions of the two blocks of soft putty have less effect on the stiffer case due to the high elastic modulus and density of the bottom. Compared with the compliant case, the homogenous case has a smaller mass density, as the result, the effect of boundary conditions of the two blocks of soft putty on crack path was smaller.

The initial kink angles are well predicted in most cases. Similar to the finding by the test, the crack kinked less when situated on the compliant side compared to the stiffer side of the FG beams that has been found numerically. However, the final crack paths derived from the phase field model can be predicted, but depend upon the impact loading profiles selected. The crack paths are found to be sensitive to the elastic functional gradient of materials.

In the contrary to quasi-static loading condition, the crack paths under dynamic loading seriously suffers the elastic wave stress exciting and altering the crack tip during the evolution of the crack. From the experimental and numerical results, it is believed that the scattered transient wave induced by impact loading has toughed the crack several times before exciting the crack to grow. As a result, the entire initiation and propagation is subjected to transient stress wave evolutions in the body. This complex oscillation of the stress waves cause difficultly in interpreting the evolution of crack paths under impact loading.

Since the original concept of the phase field fracture model is based on the energy based Griffith criterion of fracture mechanics, various energy components present in the body can hence

be explored. Here, the kinetic energy E_I, the internal elastic bulk energy E_B and the fracture energy E_C are considered, which are subsequently defined as follows [34].

$$E_I = \int_\Omega \frac{1}{2}\rho \dot{u}^2 \, dx : \text{kinetic energy} \tag{6}$$

$$E_B = \int_\Omega s^2 \psi_0(\varepsilon) dx : \text{elastic bulk energy}$$

$$E_C = \frac{G_c}{2}\int_\Omega \left(\frac{(s-1)^2}{l} + l|\nabla s|^2 \right) dx : \text{fracture energy}$$

By this way, it is possible to observe the conversion of elastic energy into kinetic and fracture energies and vice versa. Notice that the fracture energy associated with cracks is approximated by the phase field. The evolution of all the energies computed is thus depicted in Fig. 13. It is clear that the fracture energy is small compared with the kinetic and elastic energies. The elastic and kinetic energies in all cases immediately increase as soon as the point of crack initiation is reached, the fracture energy grows. The elastic bulk energy can build up in the body of specimen that is released in the fracture and kinetic energies during the propagation of the crack. As a result, the fracture energy continues to increase, whilst the elastic energy is decreased after the crack propagating. The kinetic energy is almost constant in such a way. The total energy of the system after full fragmentation of the specimen is hence approximately to be constant.

It is numerically found that the peak values of the kinetic and elastic energies of the stiffer case are almost higher than those of the compliant and homogeneous ones due to its stronger impact loading profile (Fig. 4(a)). The smaller energies of the homogeneous beam may be due to the fact that the homogeneous beam has a smaller mass density compared with that of the two FG beams. However, the impact loading profiles and the elastic gradient materials may have some influences on the fracture and kinetic energies of the body.

In terms of evolution of fracture energy, the crack initiation can be observed. It is difficult to point out exactly the time of crack initiation, however we can see that the crack initiation time increases in order of the stiffer, compliant and homogeneous cases. This observation is in consistence with experimental evidence [3]. It is worth noting that the simulation to reproduce this behavior is failed as in [10]. Regarding two FG beam configurations, although the fracture toughness at the crack tip of the stiffer is larger than that of the compliant (see Fig. 14), the crack initiation time in the stiffer case is shorter than that of the compliant case. The main reason may be attributed to the stronger loading profile applied to the stiffer case. In the compliant and homogeneous cases, the crack initiation time is found to be shorter in that of the compliant one due to its higher mass density and the lower energy fracture toughness (see Fig. 14).

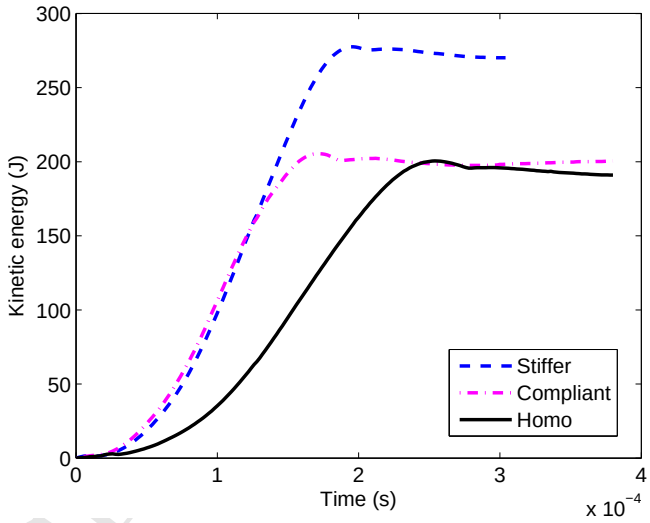

(a)

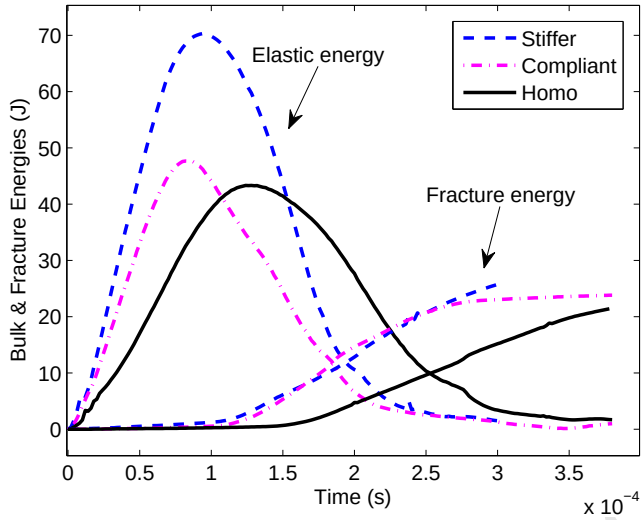

(b)

Fig. 13 Comparison of evolution of various energies in simulation of dynamic crack propagation for both FG beams and homogenous one: (a) Kinetic energy and (b) elastic bulk and fracture energies.

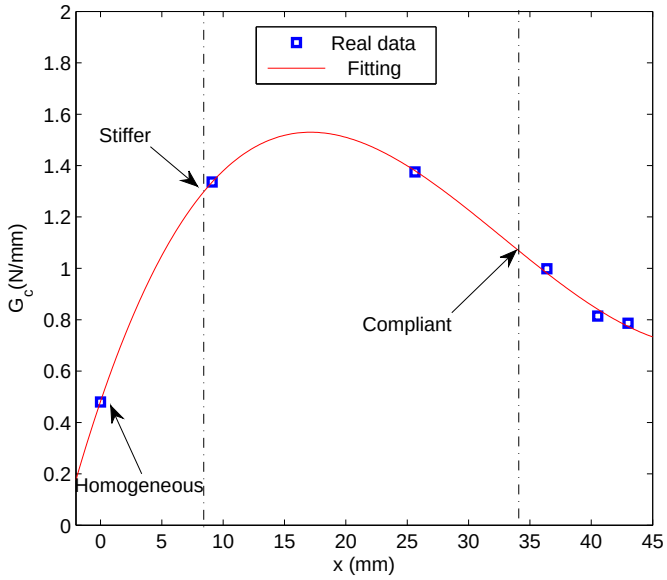

Fig. 14 Fracture toughness at the crack tip for three cases: stiffer, compliant and homogeneous.

6. Conclusions and outlook

Numerical solutions of dynamic crack propagation in FGMs with different configurations have been investigated. We adopt an effective hybrid phase field model, which is particularly suitable for

dynamic crack propagation. Works conducted particularly focus on the final crack paths, crack initiation, crack length, crack velocity, energies, etc., which are validated with respect to the experimental data. Substantially, it confirms the good performance and accuracy of the hybrid phase field approach in dynamic fracture modeling of FGMs. It is believed that the loading profiles play an important role in terms of dynamic fracture perspective. Also, the boundary conditions may affect the output results. The numerical schemes based on the phase field model can capture well the initial kink angles and the crack initiation trend regardless of materials. The initial kink angle is independent of the boundary conditions, but depends on the elastic, fracture toughness gradient and loading profiles. The hybrid phase field model taken is possible to predict well the crack paths, provided that appropriate impact loading profiles must be carefully selected. More conveniently, practices are expected to provide detailed information of loading profiles accurately, which may support well the simulations.

Nevertheless, simulation of dynamic crack propagation for other advanced composite materials and structures (e.g., FGM Al-SiC metal matrix composite with random particle [39], or cross-ply laminates in 3D [40]) with the aid of the hybrid phase field model is potential. In particular, considering the hygrothermal effects on the dynamic compressive properties of graphite/epoxy composite materials [41] or studying the vibration of FGM conical shells with mixed boundary conditions [42] using the proposed hybrid phase field approach would be very interesting.

Acknowledgments

This work was (partially) supported by the Grant-in-Aid for Scientific Research – Japan Society for the Promotion of Science (JSPS). Duc Hong Doan and Tinh Quoc Bui gratefully acknowledge the support by JSPS. Tinh Quoc Bui is also grateful to Prof. Sohichi Hirose (Director of the Department of Civil and Environmental Engineering, Tokyo Institute of Technology, Japan) for his support throughout the course of this work. The authors are also heartily grateful to Prof. Romesh C. Batra (Department of Biomedical Engineering and Mechanics, M/C 0219, Virginia Polytechnic Institute and State University, Blackburg, VA, USA) for his valuable comments and suggestions for improving the quality of the manuscript.

References

1. G.J. Nie, Z. Zhong, R.C. Batra. Material tailoring for functionally graded hollow cylinders and spheres. Compos. Sci. Tech. 71 (2011) 666-673.
2. G. Bhardwaj, I.V. Singh, B.K. Mishra, T.Q. Bui. Numerical simulation of functionally graded cracked plates using NURBS based XIGA under different loads and boundary conditions. Compos. Struct. 126 (2015) 347-359.
3. M.S. Kirugulige, H.V. Tippur. Mixed-mode dynamic crack growth in functionally graded glass-filled expoxy. Exp. Mech. 46 (2006) 269-281
4. P. Liu, T.Q. Bui, D. Zhu, T.T. Yu, J.W. Wang, S.H. Yin, S. Hirose. Buckling failure analysis of cracked functionally graded plates by a stabilized discrete shear gap extended 3-node triangular plate element. Composites Part B: Eng. 77 (2015) 179-193.
5. J. Abanto-Bueno, J. Lambros. An experimental study of mixed mode crack initiation and growth in functionally graded materials. Exper. Mech. 46 (2006) 179-196.
6. M.T. Tilbrook, B.J. Moon, M. Hoffman. Crack propagation in graded composites. Compos. Sci. Tech. 65 (2005) 201-220.
7. C. Comi, S. Mariani. Extended finite element simulation of quasi-brittle fracture in functionally graded materials. Comput. Methods Appl. Mech. Eng. 196 (2007) 4013-4026.
8. R.C. Batra, B.M. Love. Crack propagation due to brittle and ductile failures in microporous thermoelastoviscoplastic functionally graded materials. Eng. Fract. Mech. 72 (2005) 1954-1979.
9. C.E. Rousseau, H.V. Tippur. Dynamic fracture of compositionally graded materials with cracks along the elastic gradient: experiments and analysis. Mech. Mater. 33 (2001) 403-421.
10. M.S. Kirugulige, H.V. Tippur. Mixed-mode dynamic crack growth in a functionally graded particulate composite: Experimental measurements and finite element simulations. J. Appl. Mech. 75 (2008) 051102.
11. X.B. Yang, Y.P. Qin, Z. Zhuang, X.C. You. Investigation of dynamic fracture behavior in functionally graded materials. Modelling Simul. Mater. Sci. Eng. 16 (2008) 075004
12. N. Jain, A. Shukla. Mixed mode dynamic fracture in particulate reinforced functionally graded materials. Exper. Mech. 46 (2006) 137-154.
13. Z. Zhang, G. H. Paulino. Cohesive zone modeling of dynamic failure in homogeneous and functionally graded materials. Int. J. Plas. 21 (2005) 1195-1254.
14. S.S.V. Kandula, J. Abanto-Bueno, P.H. Geubelle, J. Lambros. Cohesive modeling of dynamic fracture in functionally graded materials. Int. J. Fract. 132 (2005) 275-296.
15. Z. Cheng, G. Zhang, Y. Wang, F. Bobaru. A peridynamic model for dynamic fracture in functionally graded materials. Compos. Struct. 133 (2015) 529-546.
16. A. Shukla, N. Jain, R. Chona. A review of dynamic fracture studies in functionally graded materials. Strain 43 (2007) 76-95.
17. T.L. Anderson. Fracture mechanics: Fundamentals and applications, 3rd Ed., CRC Press, Taylor & Francis, Boca Raton, 2005.
18. T.Q. Bui, Ch. Zhang. Extended finite element simulation of stationary dynamic cracks in piezoelectric solids under impact loadings. Comput. Mater. Sci. 62 (2012) 243-257.
19. T.Q. Bui, Ch. Zhang. Analysis of generalized dynamic intensity factors of cracked magnetoelectroelastic solids by X-FEM. Finite Elem. Appl. Des. 69 (2013) 19-36.
20. Z. Kang, T.Q. Bui, D.D. Nguyen, T. Saitoh, S. Hirose. An extended consecutive-interpolation quadrilateral element (XCQ4) applied to linear elastic fracture mechanics. Acta Mech. 226 (2015) 3991-4015.

21. T.Q. Bui. Extended isogeometric dynamic and static fracture analysis for cracks in piezoelectric materials using NURBS. Comput. Meth. Appl. Mech. Eng. 295 (2015) 470-509.

22. F. Armero, C. Linder. Numerical simulation of dynamic fracture using finite elements with embedded discontinuities. Int. J. Fract. 160 (2009) 119-141.

23. R.H.J. Peerlings, R. de Borst, W.A.M. Brekelmans, J.H.P. de Vree. Gradient enhanced damage for quasi-brittle materials. Int. J. Numer. Meth. Eng. 39 (1996) 3391-3403.

24. G.A. Francfort, J.J. Marigo. Revisiting brittle fracture as an energy minimization problem. J. Mech. Phys. Solids 46 (1998)1319-1342

25. C. Miehe, M. Hofacker., F. Welschinger. A phase field model for rate-independent crack propagation: robust algorithmic implementation based on operator splits. Comput Methods Appl Mech Eng 199 (2010) 2765–2778

26. M. Ambati, T. Gerasimov, L. de Lorenzis. A review on phase-field models of brittle fracture and a new fast hybrid formulation. Comput. Mech. 55 (2015) 383-405.

27. D.H. Doan, T.Q. Bui, I. Satoh, K. Fushinobu. Phase-field model for laser induced thermal crack propagation. The 52nd National Heat Transfer Symposium, Kyushu Universiyt, Kukuoka, Kyushu, Japan, 3-5, 2015.

28. B. Bourdin, C.J. Larsen, C.L. Richardson. A time-discrete model for dynamic fracture based on crack regularization. Int. J. Fract. 168 (2011) 133-143.

29. M. Hofacker, C. Miehe. Continuum phase field modeling of dynamic fracture: variational principles and staggered FE implementation. Int. J. Fract. 178 (2012) 113-129.

30. M. Hofacker, C. Miehe. A phase field model of dynamic fracture: Robust field updates for the analysis of complex crack patterns. Int. J. Numer. Meth. Eng. 93 (2013) 276-301.

31. M.J. Borden, C.V. Verhoosel, M.A. Schott, T.J.R. Hughes, C.M. Landis. A phase-field description of dynamic brittle fracture. Comput. Meth. Appl. Mech. Eng. 217-220 (2012) 77-95.

32. A. Schluter, A. Willenbucher, C. Kuhn, R. Muller. Phase field approximation of dynamic brittle fracture. Comput. Mech. 54 (2014) 1141-1161.

33. R.H.J. Peerlings, R. de Borst, W.A.M. Brekelmans, J.H.P. de Vree. Gradient enhanced damage for quasi-brittle materials. Int. J. Numer. Meth. Eng. 39 (1996) 3391-3403.

34. T. Heister, M.R. Wheeler, T. Wick. A primal-dual active set method and predictor-corrector mesh adaptivity for computing fracture propagation using a phase-field approach. Comput. Meth. Appl. Mech. Eng. 290 (2015) 466-495.

35. D.D. Nguyen, Nonlinear Static and Dynamic Stability of Functionally Graded Plates and Shells. Vietnam National University Press, Hanoi, 2014, 724 pages (Monograph)

36. V.T. Hoang, D.D. Nguyen, Nonlinear analysis of stability for functionally graded plates under mechanical and thermal loads, Compos. Struct. 92 (5) (2010), 1184-1191

37. V.T. Hoang, D.D. Nguyen, Mechanical and thermal postbuckling of higher order shear deformable functionally graded plates on elastic foundations, Compos. Struct. 93 (11) (2011), 2874-2881

38. V.T. Hoang, D.D. Nguyen, Nonlinear response of pressure-loaded functionally graded cylindrical panels with temperature effects, Compos. Struct. 92 (7) (2010), 1664-1672

39. R. Ekici, M. Kemal Apalak, M. Yildirim. Indentation behavior of functionally graded Al-SiC metal matrix composites with random particle dispersion. Compos. Part B: Eng. 42 (2011) 1497-1507.

40. I.G. Garcia, B.J. Carter, A.R. Ingraffea, V. Mantic. A numerical study of transverse cracking in cross-ply laminates by 3D finite fracture mechanics. Compos. Part B: Eng. 95 (2016) 475-486.

41. S.N Wosu, D. Hui, L. Daniel. Hygrothermal effects on the dynamic compressive properties of graphite/epoxy composite material. Compos. Part B: Eng. 43 (2012) 841-855.

42. A.H. Sofiyev, N. Kuruoglu. On a problem of the vibration of functionally graded conical shells with mixed boundary conditions. Compos. Part B: Eng. 70 (2015) 122-130.

43. H. Borouchaki, P.L. George, F. Hecht, P. Laug, E. Saltel, Delaunay mesh generation governed by metric specifications. Part I. Algorithms, Finite Elements in Analysis and Design 25 (1997) 61-83

44. H. Borouchaki, P.L. George, B. Mohammadi, Delaunay mesh generation governed by metric specifications Part II. Applications, Finite Elements in Analysis and Design 25 (1997) 85-109

45. R. El Khaoulani, P.O. Bouchard, An anisotropic mesh adaptation strategy for damage and failure in ductile materials, Finite Elements in Analysis and Design 59 (2012) 1–10